H_2 Elimination Products from Neutral Zr + Alkene Reactions in the Gas Phase

Ye Wen,† Meredith Porembski, Tricia A. Ferrett,‡ and James C. Weisshaar*

Department of Chemistry, University of Wisconsin—Madison, Madison, Wisconsin 53706-1396

Received: June 9, 1998; In Final Form: August 4, 1998

Identification of the metal-containing products of reactions of the neutral transition metal atom Zr($4d^25s^2$, ^3F) with ethylene and propylene is accomplished using one-photon ionization at 157 nm and time-of-flight mass spectrometry. The reactions proceed in a fast flow reactor at 298 K with He/N_2 buffer gas at 0.6 Torr. Mass spectra of the products of both Zr + C_2H_4 and Zr + C_3H_6 indicate that H_2 elimination occurs as the primary reaction step. The efficiency of the Zr + C_2H_4 reaction shows that there is no barrier larger than about 2 kcal/mol above reactants along the entire reaction path. This corroborates an earlier theoretical prediction by Blomberg and Siegbahn of facile H_2 elimination by ground-state Zr. For the secondary reactions ZrC_2H_2 + C_2H_4 and ZrC_3H_4 + C_3H_6 and for the reactions ZrO + C_2H_4 and ZrO + C_3H_6, mass spectra again indicate that H_2 elimination occurs. Rate constant measurements using photoionization detection show that the presence of the C_2H_2 and C_3H_4 ligands enhances the reaction efficiency over that of the bare Zr atom, while ZrO reacts at essentially the same rate as Zr.

I. Introduction

The gas-phase transition-metal atoms M and M^+ provide an organometallic model chemistry involving substantial electronic complexity but lacking the additional burden of ligands and solvents.[1−3] Like typical solution-phase organometallic reactions, *neutral* M + hydrocarbon reactions in the gas phase often involve potential energy barriers. We have extensively surveyed the chemical reaction kinetics of ground state neutral transition-metal atoms from the 3d, 4d, and 5d series with small alkanes and alkenes.[4−8] Several other groups have also studied reactions of neutral metal atoms and clusters with oxidants and hydrocarbons in flow reactors[9−15,16−19] and most recently in crossed beams.[20] Our work has been carried out in a fast flow reactor with 0.4−1.2 Torr He buffer gas using laser-induced fluorescence (LIF) to monitor the decay of metal atom density vs hydrocarbon flow. Although only a few of the atoms studied (for example, Rh, Pd, and Pt) were found to react with alkanes, most of the atoms, including Zr, react with alkenes.

Such kinetics data allow quantitative comparisons with modern electronic structure theory.[8,21−26] However, thus far, we have determined neither the mass nor the structure of the products directly. In a few cases, the bimolecular rate constant increases significantly with He pressure, which indicates that termolecular stabilization of long-lived M(hydrocarbon) complexes contributes to the removal of M. In most cases, the absence of a pressure dependence of the measured rate constant over the limited range 0.4−1.2 Torr suggests, *but does not prove*, that bimolecular elimination occurs. Especially for M + alkene reactants, which typically fall into a deep M(alkene) complex well, it is possible that essentially all such complexes are so long-lived (perhaps 200 ns or longer) that termolecular stabilization occurs with unit efficiency over the limited range of pressures studied, 0.4−1.2 Torr. The reaction efficiency would then measure only the probability per collision that reactants in fact reach the deep complex well.

Using the scaled configuration interaction method named PCI-80, Blomberg, Siegbahn, and Svensson[8] predicted that the ground-state Nb and Zr + C_2H_4 reactions proceed by formation of a long-lived M(C_2H_4) complex, insertion by the metal into a CH bond, and subsequent rearrangement and elimination of H_2. For Zr, evidently the largest barrier along the entire pathway involves the CH insertion step, whose transition state lies only 1.8 kcal/mol above the reactants. The purpose of this paper is to test the prediction that ground-state Zr($4d^25s^2$) can effect bimolecular H_2 elimination from small alkenes at 298 K. We accomplish this by one-photon ionization of the products at 157 nm (7.9 eV) and time-of-flight mass analysis of the resulting cations. For Zr + C_2H_4 and Zr + C_3H_6, we observe cations of stoichiometry $ZrC_2H_2^+$ and $ZrC_3H_4^+$, respectively. We argue in detail that these are indeed parent cations, so the new results corroborate a significant theoretical prediction. Recently, Mitchell, Hackett, and co-workers[27] have used a similar technique with 193 nm ionization to study the kinetics of Mo clusters, whose ionization energy is lower. Very recently, the Davis group has studied the same Zr + C_2H_4 reaction by crossed beams, and they also observe $ZrC_2H_2^+$ by 157 nm photoionization.[28]

The same photoionization scheme can measure rate constants of both bare and partially ligated metal atoms; the latter usually cannot be studied by LIF. Here, we present new rate constants for the reactions Zr(C_2H_2) + C_2H_4, Zr(C_3H_4) + C_3H_6, ZrO + C_2H_4, and ZrO + C_3H_6 at 298 K. In all four cases, photoionization again indicates bimolecular H_2 elimination as the dominant reaction path.

II. Experimental Section

The modular fast flow reactor (schematic in Figure 1) consists of a source region, a reaction zone, and a detection zone. It has been used in the past for studies of ground-state kinetics of M and M^+ formed by laser ablation or a hollow cathode discharge and detected by LIF or quadrupole mass spectrometry.[4−8,10,11,21,29,30] Recently, we have used stimulated

* To whom correspondence should be addressed. Email: weisshaar@chem.wisc.edu.

† Current address: KLA-Tencor Corp., One Technology Drive, Milpitas, CA 95035.

‡ Permanent address: Carleton College, Department of Chemistry, 1 N. College Street, Northfield, MN 55057.

10.1021/jp9825617 CCC: $15.00
Published on Web 10/02/1998

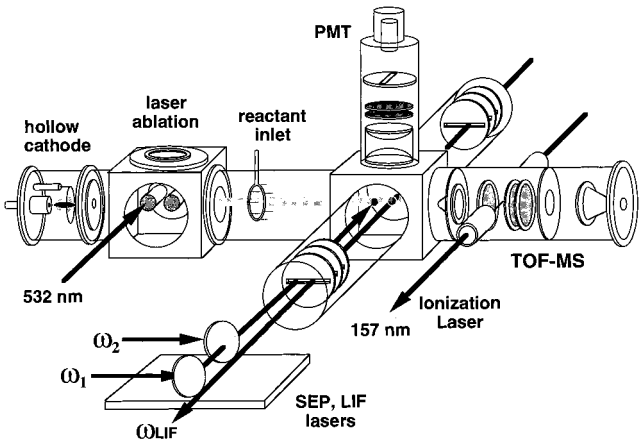

Figure 1. Schematic of fast flow reactor including hollow cathode discharge and laser ablation sources of transition-metal atoms, reactant inlet, dye lasers used for stimulated emission pumping (ω_1 and ω_2) and laser-induced fluorescence (ω_{LIF}), photomultiplier tube for LIF detection, and time-of-flight mass spectrometer (TOF-MS, not to scale) using 157 nm excimer laser photoionization.

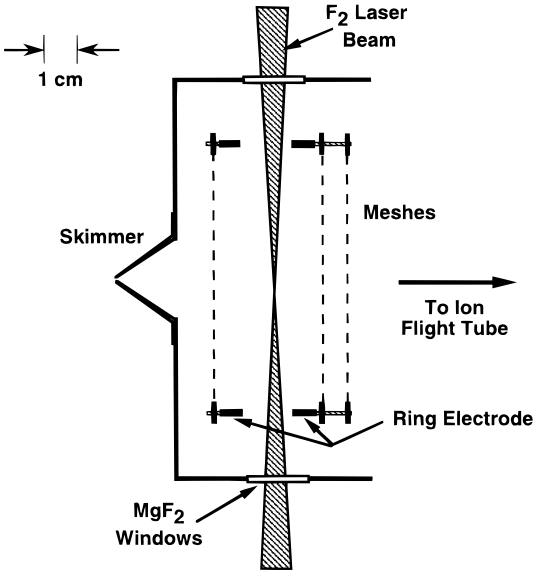

Figure 2. Schematic of photoionization region, roughly to scale.

emission pumping to study the kinetics of V* and Mo* excited electronic states.[31,32]

In the current work, a laser vaporization source (Nd:YAG harmonic at 532 nm, 10 ns fwhm) produces gas-phase Zr atoms upstream in a fast flow of predominantly He (typically 0.56 Torr) and some N_2 (typically 60 mTorr) buffer gas. The N_2 is added to quench He* and Zr* metastable states. We know from previous work using LIF[10] that laser vaporization makes larger peak number densities of metal atoms but a substantially greater fraction of excited states M* than the continuous sputtering source that had become our standard for simple rate constant measurements. Since the photoionization detection is not state-specific, we will consider possible effects of these excited states on the observed kinetics and product identity. The measured mean bulk flow speed of He is 5400 cm/s in the reaction region. On the basis of earlier calibrations with neutral Ti,[4] we expect a factor of 1.45 between the bulk flow speed and the mean speed of transport of neutral Zr down the flow tube. Thus, we take $\bar{v} = 7800 \pm 600$ cm/s for all transition metal species. As argued in detail earlier,[7] assuming a hard-spheres model holds reasonably well for the diffusion of molecular species such as Ti, Zr, ZrO, ZrC_2H_2, and ZrC_3H_4 in He, we expect all such species to be transported down the flow tube at the same mean speed within about ±15%. A detailed study of the transport of different species down the flow tube is underway.

The hydrocarbon gas is added midstream through a showerhead inlet oriented upstream relative to the He flow. The distance from laser vaporization source to the hydrocarbon gas inlet is typically 45 cm. The reaction zone extends from the gas inlet to the skimmer that samples neutrals into the detection region, a length of 52 cm in this work. The temperature in the middle of the reaction zone 74 cm downstream of the source is 298 ± 5 K. Flow of hydrocarbon is regulated by a needle valve or a flow controller and monitored by a mass flow meter (Tylan). The hydrocarbon gases ethylene (Matheson, >99.5%) and propylene (Matheson or Liquid Carbonic, >99.0%) were used directly from the bottle. Because flow meter response is not linear with gas flow, we have directly calibrated the flow meters for each reactant gas.

In earlier work we used LIF to monitor the decay of the metal atom concentration vs hydrocarbon number density, measuring effective bimolecular rate constants for reactions of ground-state M.[7] In this work, we add the ability to identify the products using one-photon ionization at 157 nm (F_2 laser, 7.9 eV) and time-of-flight mass spectrometry (TOF-MS). The geometry of the ionization region is shown schematically in Figure 2. The skimmer is a home-built thin brass cone with a sampling orifice of 1.3 mm diameter. The skimmer and its flange are electrically isolated and floated at +100 VDC relative to the flow tube to prevent ions formed in the ablation source from entering the TOF-MS. Ions formed by the ionization laser travel 1.7 cm in the first extraction field, 0.9 cm in the second extraction field, and then 41 cm in field-free flight to the microchannel plate detector. Mass spectra are digitized as the voltage drop over a 50 Ω load vs time in a digital oscilloscope (Lecroy 9310M). Typically, 1000 traces are averaged.

Voltages on the three meshes forming the Wiley−McLaren extraction region are +2500, +1460, and 0 V. It was necessary to pulse the positive voltages using a dual thyratron circuit. The leading edge of the voltage pulse defines $t = 0$ for the TOF-MS. When using dc voltages, we observed very large ion peaks due to He^+ and N_2^+ but no signal from Zr^+, perhaps because of a discharge through the activated gas. The voltage pulses are applied 100 ns after the ionizing laser pulse. The voltages rise to 95% of their height in 25 ns, remain flat for some 10 μs, and then decay to zero in 75 μs. The ring electrode (Figure 2) is pulsed to a value halfway between the two positive meshes, which helps to flatten the fields in the ion extraction region and may even be used as a mild electrostatic lens to improve ion collection efficiency. Ion peak widths are 20−30 ns fwhm when the extraction voltages are optimized, corresponding to a mass resolution $m/\delta m$ of about 150.

Immediately after a fresh gas fill, the F_2 laser (Lumonics, model 500) typically provides 3 mJ/pulse as measured with a Gentec joule meter (ED-200) after two reflections from dielectric mirrors and traversal of a 2.7 m long tube purged with N_2 gas. The laser is collimated by a 44 cm focal length MgF_2 lens positioned 36 cm from the center of the ionization volume. The laser enters the ionization region through two MgF_2 windows. The lens focuses the beam to the smallest spot size some 8 cm beyond the ionization volume. As a rough estimate, at the center of the ionization volume the laser spot is a 3 mm × 8 mm rectangle with its long side parallel to the axis of the TOF-MS. Shot-to-shot fluctuations of the laser pulse energy are typically ±12%. After a fresh gas fill, the pulse energy decays exponentially in time with a 1/e decay rate of 0.021 min^{-1}.

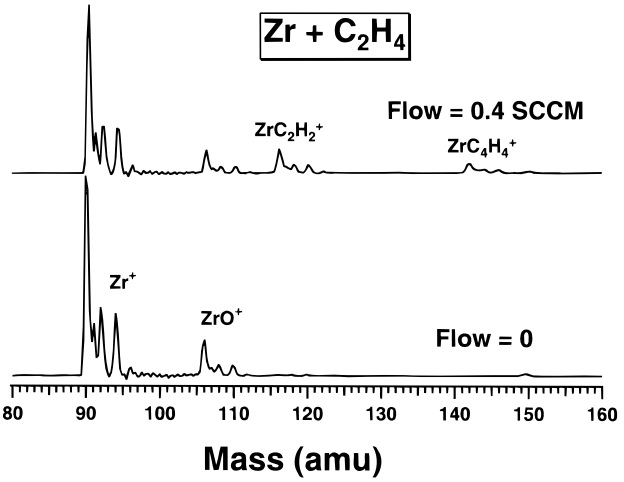

Figure 3. Time-of-flight mass spectra with Zr target with and without ethylene flow as indicated.

Zr, Ti, and Mo atoms all seemed comparably easy to produce and ionize. The integrated current from an optimized signal from photoionization of Zr corresponds to about 400 Zr^+ ions per shot at the detector. We see a substantial amount of He^+, N^+, and N_2^+ at low mass as well as peaks due to diffusion pump oil that can interfere with the transition-metal species of interest. With ethylene as reactant, the mass spectra include peaks due to Zr^+, $ZrC_2H_2^+$, and $ZrC_4H_4^+$, as well as an impurity ZrO^+ peak unrelated to ethylene flow.

Collisions between metal species and ethylene end quite abruptly at the skimmer, and the effective reaction length z is taken as the distance from the hydrocarbon inlet to the skimmer, 52 cm. In the main flow tube at 0.6 Torr buffer gas, the mean free path between hard spheres collisions is about 0.2 mm. Flow through the 1.3 mm diam skimmer thus lies in the transition region between viscous and molecular flow. The He density decreases rapidly from about 2×10^{16} cm^{-3} at the skimmer to about 10^{12} cm^{-3} at the point of laser photoionization 5 cm further downstream. The probability of a Langevin collision between a photoion and a hydrocarbon molecule during extraction is less than 0.01%. The probability of a Langevin collision between a photoion and a He atom is less than 0.2%. Thus, the mass spectrum should include only photoions formed by interaction with the laser in collision-free conditions. No subsequent bimolecular ion−hydrocarbon collisions can produce secondary product ions en route to the detector, and there should be no collision-induced dissociation of molecular photoions.

In the next section we describe the use of the ion signals to remeasure the effective bimolecular rate constant for ground-state Zr + alkene collisions, to identify the products of that first step as $ZrC_2H_2 + H_2$ rather than a collisionally stabilized adduct ZrC_2H_4, to measure the effective bimolecular rate constant for the secondary reaction Zr(acetylene) + alkene, and to identify the secondary products as the complexes $Zr(alkyne)_2 + H_2$ rather than a mixed adduct of the form Zr(alkyne)(alkene).

III. Results

During a typical experiment, hydrocarbon flow was varied between 0 and 6.5 sccm (standard cm^3/min) while He and N_2 flows were maintained at 10 000 and 970 sccm, respectively. These conditions correspond to number densities of 10^{16} cm^{-3} He, 10^{15} cm^{-3} N_2, and between 0 and 10^{13} cm^{-3} hydrocarbon.

For the $Zr + C_2H_4$ reaction sequence, Figure 3 shows typical photoionization mass spectra taken with zero ethylene flow and 0.4 sccm of ethylene flow. At zero flow, we observe Zr^+ and ZrO^+; the latter could be from reaction of Zr with O_2 impurity or more likely from ZrO ablated from the oxidized metal surface. The Zr isotope intensity pattern at 90, 91, 92, 94, and 96 amu is in good accord with natural abundances of 51%, 12%, 17%, 17%, and 3%, respectively. As ethylene flow increases, both Zr^+ and ZrO^+ signals decrease. The ions $ZrC_2H_2^+$ and $ZrC_4H_4^+$ rise roughly simultaneously. At the largest flow studied, 6.5 sccm, Zr^+, $ZrC_2H_2^+$, and ZrO^+ are essentially gone while $ZrC_4H_4^+$ persists. When the ZrO^+ impurity peak is particularly strong, we see small product peaks at the proper masses for $ZrOC_2H_2^+$ and $ZrOC_4H_4^+$. Ground-state ZrO evidently reacts with ethylene to form products that are not as readily ionized by the 157 nm laser perhaps because the ionization energy is too large.

The simplest interpretation of data like that of Figure 3, confirmed by detailed kinetic analysis below, is that ground-state Zr undergoes the sequential H_2 elimination reactions:

$$Zr + C_2H_4 \xrightarrow{k_1} ZrC_2H_2 + H_2 \quad (1)$$

$$ZrC_2H_2 + C_2H_4 \xrightarrow{k_2} ZrC_4H_4 + H_2 \quad (2)$$

We see no evidence in the mass spectra for formation of collisionally stabilized adducts of stoichiometry ZrC_2H_4 or ZrC_4H_8. For example, a small contribution from $ZrC_2H_4^+$ would appear as an enhancement of the $^{92}ZrC_2H_2^+$ peak and especially of the minor $^{96}ZrC_2H_2^+$ peak in the mass spectrum compared with the isotope pattern for pure Zr^+. We estimate that the contribution of $ZrC_2H_4^+$ to the region 116−124 amu cannot be larger than 10% of the contribution from $ZrC_2H_2^+$. Similarly, the combined contribution of $ZrC_4H_6^+$ and $ZrC_4H_8^+$ to the region 142−150 amu cannot be larger than 10% of the contribution from $ZrC_4H_8^+$. The substantial peak at 150 amu is background due to ionization of pump oil; it appears in the absence of ethylene. Previously, the $Zr + C_2H_4$ reaction was examined at total flow tube pressures of 0.5 and 0.8 Torr. In that study,[6] the observed invariance of the rate constant with pressure further supports a mechanism of H_2 elimination for this reaction.

We know that the ZrC_2H_2 and ZrC_4H_4 products arise from $Zr + C_2H_4$ collisions rather than impurity $ZrO + C_2H_4$ collisions because the relative abundance of ZrO varies substantially from day to day while the ratio of product signal to Zr signal does not. The experiment provides no evidence that the structure of the species ZrC_2H_2 is a distorted acetylene molecule complexed to the metal atom, but theory suggests this is so. Similarly, we have no experimental evidence that ZrC_4H_4 is the diacetylene complex $Zr(C_2H_2)_2$, but this also seems likely.

Integration of the largest isotope peaks for Zr^+ and $ZrC_2H_2^+$ gives kinetics plots of ion signal vs ethylene number density such as those in Figure 4. These data are corrected for the systematic decay of the ionizing laser intensity by periodically remeasuring the Zr^+ signal in the absence of hydrocarbon flow and interpolating a correction factor. We analyzed the data according to the sequential, bimolecular kinetics scheme of eqs 1 and 2. The solution to this model is the time-honored:

$$[Zr] = [Zr]_0 \exp(-k_1 n_{hc} z_{rxn}/\bar{v}) \quad (3)$$

$$[ZrA] = \frac{[Zr]_0 k_1}{k_2 - k_1}[\exp(-k_1 n_{hc} z_{rxn}/\bar{v}) - \exp(-k_2 n_{hc} z_{rxn}/\bar{v})] \quad (4)$$

Here, [Zr] is the Zr atom density, [ZrA] is the ZrC_2H_2 density

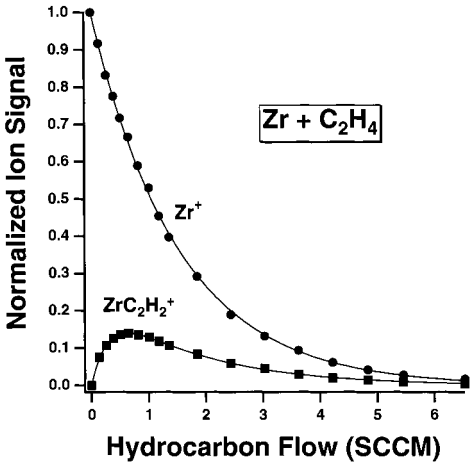

Figure 4. Integrated ion currents for Zr^+ and $ZrC_2H_2^+$ peaks for Zr + C_2H_4 reaction, normalized for the decay of 157 nm laser intensity and plotted vs ethylene flow; 1 sccm produces a number density of 2×10^{12} cm^{-3}.

TABLE 1: Effective Bimolecular Reaction Rates in 0.06 Torr N_2 and 0.56 Torr He at 298 ± 5 K

reaction	rate constant (10^{-12} cm^3 s^{-1})[a]	primary product stoichiometry[b]
$Zr + C_2H_4$	55 ± 16	$ZrC_2H_2 + H_2$
$Zr + C_3H_6$	135 ± 40	$ZrC_3H_4 + H_2$
$ZrC_2H_2 + C_2H_4$	280 ± 140	$ZrC_4H_4 + H_2$
$ZrC_3H_4 + C_3H_6$	230 ± 110	$ZrC_6H_8 + H_2$
$ZrO + C_2H_4$	59 ± 18	$ZrOC_2H_2 + H_2$
$ZrO + C_3H_6$	175 ± 50	$ZrOC_3H_4 + H_2$

[a] Uncertainties reflect possible systematic errors in reaction time, flow calibrations, etc., as well as the fitting procedure; see text for details. Earlier work (ref 6) found (59 ± 12) × 10^{-12} and (149 ± 30) × 10^{-12} for $Zr(^3F_2)$ reaction with C_2H_4 and C_3H_6, respectively, in 0.44 Torr He, 0.06 Torr N_2, and 0.003 Torr Ar buffer gases using LIF detection. [b] Metal-containing product inferred from photoionization mass spectrum assuming only parent cations, as argued in the text. H_2 product follows from approximate thermochemistry and mass balance.

(with A denoting acetylene), k_1 and k_2 are defined in eqs 1 and 2, n_{hc} is hydrocarbon number density, z_{rxn} is the reaction length of 52 cm, and $\bar{v}$ = 7800 cm/s is the mean speed of metal-containing species down the flow tube. We assume the same $\bar{v}$ for Zr and ZrA,[7] although the data suggest this may only be true to about 15%.

First, we fit the decay of the Zr^+ signal vs n_{hc} to eq 3 in a least-squares sense to extract the best-fit value of k_1. In fitting the rising and falling $ZrC_2H_2^+$ signal to eq 4, we froze k_1 at the best-fit value obtained from the Zr^+ data. The resulting best-fit functions are shown as the solid lines in Figure 4. The best-fit values of k_1 and k_2 are given in Table 1 as averages over the results from two separate experiments. This new value of k_1 = (55 ± 16) × 10^{-12} cm^3 s^{-1} in 0.56 Torr He and 60 mTorr N_2 from photoionization of Zr compares favorably with the older value[6] of (59 ± 12) × 10^{-12} cm^3 s^{-1} in 0.44 Torr He, 60 mTorr N_2, and 3 mTorr Ar buffer gas from electronic state-specific LIF detection of ground-state $Zr(^3F_2)$.

The fit to the $ZrC_2H_2^+$ signal with k_1 frozen at the value derived from the Zr^+ decay shows a slight systematic error in the flow range 2−5 sccm. As an alternative, we used the best-fit values from the above procedure as initial guesses in unconstrained fits in which both k_1 and k_2 were adjustable parameters. For example, in the data set shown in Figure 4, the unconstrained procedure gave $k_1 = 48 \times 10^{-12}$ cm^3 s^{-1} and $k_2 = 285 \times 10^{-12}$ cm^3 s^{-1} compared with $k_1 = 56 \times 10^{-12}$ cm^3 s^{-1} from the Zr^+ data and $k_2 = 243 \times 10^{-12}$ cm^3 s^{-1} from the constrained fit to the $ZrC_2H_2^+$ data. The unconstrained procedure reduces χ^2 by a factor of 3, which is significant. Both procedures define the best-fit parameters quite sharply as judged by diagonal and off-diagonal covariance matrix elements, but the unconstrained fit is clearly more satisfactory. The systematic difference between the two procedures may be due to real differences in the transport of Zr and ZrC_2H_2 down the flow tube due to different diffusion coefficients in He. In practice, we used the constrained procedure to obtain the secondary rate constants.

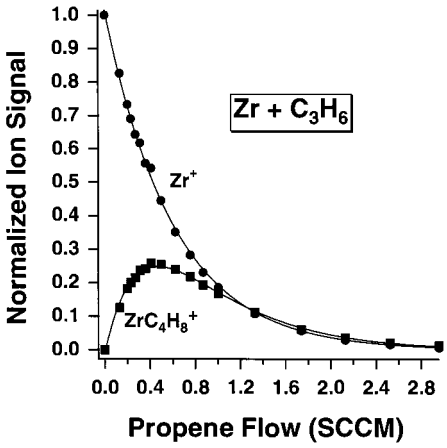

Figure 5. Integrated ion currents for Zr^+ and $ZrC_3H_4^+$ peaks for Zr + C_3H_6 reaction, normalized for the decay of 157 nm laser intensity and plotted vs propylene flow; 1 sccm produces a number density of 2×10^{12} cm^{-3}.

In Table 1 the ±30% error estimates on the primary reaction rates (k_1 and k_5 below) arise predominantly from uncertainties in the mean reaction time, flow calibrations, etc. The ±50% error estimates on the secondary reaction rates (k_2 and k_6 below) include the additional possible systematic error from uncertainties in the fitting procedure (evidently on the order of 15−25%). We are carrying out a detailed study of arrival time distributions of different species in the flow tube, which may eventually allow us to refine our analysis.

For the Zr + propylene reaction, analogous mass spectra again point to sequential elimination of two H_2 molecules:

$$Zr + C_3H_6 \xrightarrow{k_5} ZrC_3H_4 + H_2 \quad (5)$$

$$ZrC_3H_4 + C_2H_4 \xrightarrow{k_6} ZrC_6H_8 + H_2 \quad (6)$$

These photoionization mass spectra are not shown. The kinetics data are plotted in Figure 5. An analogous kinetics scheme was applied in the same fashion, leading to the best-fit functions shown as the solid lines and the values of k_5 and k_6 for the sequential propene reactions collected in Table 1. Again, the constrained procedure was used to fit the $ZrC_3H_4^+$ signals, and again, unconstrained fits suggest possible additional systematic errors on the order of 15−25%. The new value of k_5 = (135 ± 40) × 10^{-12} cm^3 s^{-1} in 0.56 Torr He and 60 mTorr N_2 from photoionization agrees well with the older value[6] of (149 ± 30) × 10^{-12} in 0.44 Torr He, 60 mTorr N_2, and 3 mTorr Ar from LIF detection of the $Zr(^3F_2)$ ground state. The latter study also found this rate constant to be independent of pressure over the limited range between 0.5 and 0.8 Torr.

We also successfully fit single-exponential models to the decay of ZrO^+ ion signals vs both C_2H_4 and C_3H_6 density. Typically, no ions associated with products appeared in either

case, but weak signals at masses corresponding to H_2 elimination were observed whenever the ZrO^+ signal was particularly strong. The primary reaction rate constants for $ZrO + C_2H_4$ and $ZrO + C_3H_6$ are included in Table 1.

IV. Discussion

A. Product Identification. Before discussion of reaction mechanisms, it is important to explain in detail why we believe our photoionization experiment is detecting *parent cations* from *single-photon ionization* of the neutral ZrC_2H_2 and ZrC_3H_4 products of the reactions of Zr in its *ground electronic state*. Several alternative possibilities must be examined critically. First, the ground-state cation Zr^+ itself undergoes exothermic H_2 elimination reactions with alkenes, but we have already ruled out the possibility that Zr^+ from photoionization of Zr reacts in the ionization region to produce the observed $ZrC_2H_2^+$ ions on the basis of number density considerations and the Langevin cross section.

Second, we know from LIF spectra that the laser ablation source makes Zr atoms in both the ground state ($4d^25s^2$, ^3F) and a variety of excited states. Low-lying $d^{x-1}s^1$ and $d^{x-2}s^2$ states have the same even parity as the ground state. It is imaginable that we are observing products only from the excited-state reactions. Such states are highly metastable with respect to radiative decay but will be quenched to the ground state by collisions with He, N_2, and added hydrocarbon in the flow tube.

In earlier work using a laser ablation source of Ti, Ritter and co-workers[10] estimated that excited states comprised less than 10% of the total population 35−45 cm downstream from the ablation source. In our early photoionization work, the point of hydrocarbon addition was only 20 cm downstream from the source. In that geometry, excited states of Zr evidently do manifest themselves in the kinetics plots of Zr^+ signal vs alkene flow as deviations from the single-exponential decay predicted by eq 3. The degree of these deviations depended quite sensitively on experimental conditions, including the ablation laser pulse energy and the distance between ablation source and point of hydrocarbon addition. We saw greater positive curvature in plots of $\ln(Zr^+)$ vs n_{hc} with increasing ablation energy and with decreasing distance between the points of ablation and alkene addition, as expected for contributions from excited states. Within experimental error, the slow-decay component of the nonexponential decays observed at smaller source-hydrocarbon inlet distance matches the single-exponential rate observed for longer distances (Figures 4 and 5), further suggesting that the fast decay is due to excited-state reactions and the slow decay is due to ground-state reaction. The product mass spectra are the same, independent of distance between source and inlet. This suggests that the unidentified Zr* excited state(s) produce the same H_2 elimination products as the ground state.

All of the final results reported here were obtained with the distance increased to 45 cm between the Zr source and the point of hydrocarbon addition. In that geometry, the decay of the Zr^+ signal becomes exponential vs alkene flow (Figures 4 and 5). Under these same conditions, the measured rate constants for $Zr + C_2H_4$ and $Zr + C_3H_6$ agree within error limits with the *ground-state-specific* Zr + alkene rate constants measured previously using LIF detection,[6] as described in the footnote to Table 1. This combined evidence allows us to conclude unambiguously that ground-state Zr reacts with ethylene and propene at 298 K in 0.6 Torr buffer gas to make a neutral product that yields the ions $ZrC_2H_2^+$ and $ZrC_3H_4^+$, respectively, on photoionization at 157 nm.

We also believe that one-photon rather than two-photon ionization processes dominate the production of all ions for several related reasons. First, the estimated photon fluence is at most 10^{16} photon/cm^2 with a fresh laser fill, much smaller than the reciprocal of a typical photoionization or photodissociation cross section of $10^{-17}-10^{-18}$ cm^2. For such cross sections, one-photon ionization followed by one-photon fragmentation of the parent cation will be a rare event. Second, fluctuations in the photoionization signal seem to be directly proportional to those of the laser pulse energy, whereas in a two-photon process they might be expected to be more severe. Finally, the species present in the mass spectrum do not change with laser fluence over at least a factor of 10, as measured over the natural course of a particular fill of laser gases.

A final undesirable possibility is that the mass spectrum involves *fragment ions* rather than parent cations of the neutral reaction products. Perhaps the neutral products are exclusively the collisionally stabilized adduct (ZrC_2H_4 or ZrC_3H_6), and such adducts produce 100% fragment ions (loss of H_2) on photoionization at 157 nm (7.9 eV). Theory[21] indicates that the $Zr + C_2H_4$ reaction proceeds through a deep $Zr(C_2H_4)$ complex well whose minimum lies some 38 kcal/mol = 1.65 eV below reactants, including differential effects of zero-point energy. Neither the adiabatic ionization energy $IE(ZrC_2H_4)$ nor the cation dissociation energy $D_0(Zr^+-C_2H_4)$ are known, but they are related to the known IE(Zr) = 6.84 eV[33] by the cycle

$$IE(ZrC_2H_4) - IE(Zr) = D_0(Zr-C_2H_4) - D_0(Zr^+-C_2H_4) \quad (7)$$

Using the estimate $D_0(Zr-C_2H_4) = 1.65$ eV from electronic structure theory and estimating $D_0(Zr^+-C_2H_4)$ as being equal to the experimentally known value of $D_0(Ti^+-C_2H_4) = 1.51$ eV,[34] we obtain a rough estimate of $IE(ZrC_2H_4) \approx 7.0$ eV. A single 7.9 eV photon might thus deposit as much as about 0.9 eV of internal energy in $ZrC_2H_4^+$. The energy of $ZrC_2H_2^+ + H_2$ is also unknown. In the isoelectronic case $Ti^+ + C_2H_4 \rightarrow TiC_2H_2^+ + H_2$, the exothermicity is 0.8 eV from experimental thermochemistry.[34] We therefore expect $ZrC_2H_2^+ + H_2$ to lie about 0.8−1.0 eV below $Zr^+ + C_2H_4$, or about 0.2−0.4 eV below the *maximum possible* energy available from photoionization. The larger numbers in each range allow for the possibility that the strengths of bonds to Zr^+ are as much as 0.2 eV larger than those to Ti^+.

It is thus probably *barely energetically feasible* for photoionization of ZrC_2H_4 at 7.9 eV to produce $ZrC_2H_4^+$ with sufficient internal energy to fragment to $ZrC_2H_2^+ + H_2$, but *only if photoionization deposited almost all of the available energy into internal energy of the parent ion* rather than into kinetic energy of the photoelectron. This is highly unlikely. Electronic structure calculations indicate that both ZrC_2H_4 and $ZrC_2H_4^+$ lie in deep potential wells of similar geometry. The strong Franck−Condon propensity will then be to form internally quite cold $ZrC_2H_4^+$ cations from room-temperature ZrC_2H_4. In addition, a substantial barrier likely separates the $ZrC_2H_4^+$ adduct from $ZrC_2H_2^+ + H_2$ elimination products, so we would expect almost all of the $ZrC_2H_4^+$ cations from photoionization of a 298 K sample to remain chemically stable. Since *no* $ZrC_2H_4^+$ cations are observed, the substantial $ZrC_2H_2^+$ signal almost surely arises from photoionization of ZrC_2H_2 products of the neutral reaction. The same arguments hold for the $ZrC_3H_4^+$ cations observed in the $Zr + C_3H_6$ reaction, which almost surely are parent cations of ZrC_3H_4 products. Recent results from crossed-beam work in the Davis group[28] are in agreement. Under single-collision reaction conditions, they also

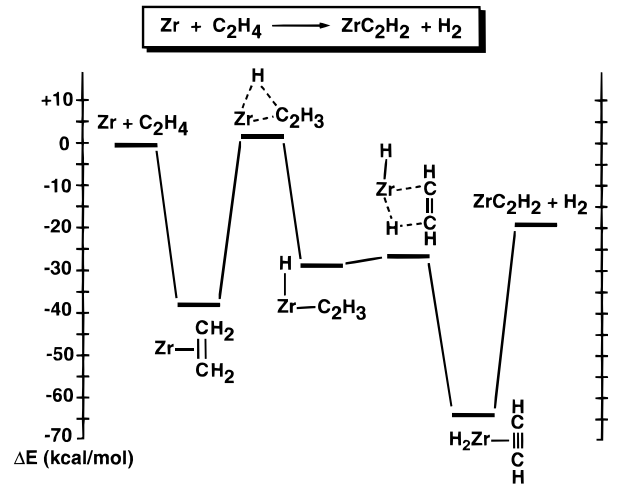

Figure 6. Theoretical stationary point energies along lowest energy Zr + C_2H_4 reaction path from Blomberg and Siegbahn (ref 8) using PCI-80 method. Energies are corrected for differential zero-point effects estimated from harmonic frequencies.

observe $ZrC_2H_2^+$ from 157 nm photoionization of the products of Zr + C_2H_4.

There remains the nagging possibility that in our flow-tube experiment we are observing the *minority product*; i.e., that both Zr + alkene reactions in 0.6 Torr buffer gas produce *primarily* collisionally stabilized Zr(alkene) adducts, but these adducts happen to have an unusually small photoionization cross section at 7.9 eV. The Zr(alkyne) products could have unusually *large* photoionization cross sections as well. The best way to test this possibility will be to make the Zr(alkene) adducts directly in ligand exchange reactions and to attempt to photoionize them in our apparatus. We are pursuing that experimental avenue. In the meantime, we can conclude with confidence that ground-state Zr produces at least *some* H_2 elimination products in reactions with ethylene and propylene at 298 K.

B. Reaction Mechanisms. Stationary points along the adiabatic potential energy profile (lowest energy *triplet* surface) for the Zr + C_2H_4 → ZrC_2H_2 + H_2 reaction calculated by Blomberg, Siegbahn, and Svensson[21] are reproduced in Figure 6. These energies come from scaled configuration interaction calculations using the method known as PCI-80; they include harmonic corrections for zero-point energies. The theoretical reaction path involves addition of the Zr($4d^25s^2$, ^3F) ground state to the CC double bond to form a triplet metallocyclopropane intermediate in a deep potential well. The calculated barrier to CH insertion from this well lies 1.8 kcal/mol above reactants. The Zr(H)(C_2H_3) intermediate, which lies 28.7 kcal/mol below reactants, rearranges easily to the very deep exit-channel complex Zr(H)$_2$(C_2H_2), which lies some 63 kcal/mol below reactants and eliminates H_2 without any additional barrier. There is another, more weakly bound Zr(C_2H_4) species on the lowest *quintet* surface, but it probably plays little or no role in the ground-state triplet chemistry.

The calculations did not explore the possibility of an *entrance channel barrier* on the adiabatic triplet surface lying between Zr($4d^25s^2$, ^3F) + C_2H_4 and the triplet Zr(C_2H_4) well. Chemical intuition suggests there might be such a barrier due to repulsive forces between the closed-shell $5s^2$ "outer configuration" of the metal atom and the closed-shell alkene. However, experiment shows that the total removal rate of Zr in collisions with C_2H_4 is about 20% of the estimated hard-spheres collision rate at 298 K. The simple Arrhenius expression with the preexponential taken to be equal to the hard-spheres rate then indicates that there can be no barrier to reaction larger than about 2 kcal/mol.

Remarkably, the Zr($4d^25s^2$, ^3F) ground-state atom is evidently able to hybridize to a $4d^2(sd_-)^2(sd_+)^0$ configuration quite early in the collision with little energetic cost.[35,36] Here sd_+ and sd_- are symmetric and antisymmetric combinations of the 5sσ and 4dσ orbitals on Zr, which maximize probability density on the Zr−ethylene approach axis and in a plane perpendicular to it, respectively. The compensating attractive force involves the donor−acceptor interaction from π^2 on ethylene into the empty sd_+ orbital on the metal. The net effect is little or no barrier to addition to the double bond.

Our new photoionization results thus corroborate the theoretical prediction that ground-state Zr + C_2H_4 reactants can proceed to H_2 elimination products with at most a small barrier. Neither experiment nor theory yet addresses the issue of whether the reaction efficiency is low because of a small entrance channel barrier on the triplet surface, a small subsequent barrier to CH insertion, or some combination of these. The role of angular momentum conservation in passage over the CH insertion barrier may also be important.[37]

We hope to gain further insight into these subtle issues by studying the reaction rate vs temperature and by using the new photoionization technique to study the Zr + C_2D_4 reaction as well. Statistical modeling using geometries and harmonic frequencies from electronic structure theory may then allow for determination of the exact location of the key barrier.

Finally, we can begin to compare the reaction rates of the partially ligated species ZrO, ZrC_2H_2, and ZrC_3H_4 with alkenes to those of ground-state Zr itself. The ZrO rates are remarkably similar to the Zr rates, while the ZrC_2H_2 and ZrC_3H_4 rates are substantially faster, approaching the hard-spheres limit of unit reaction probability. The ZrO molecule is strongly bound by what is most simply viewed as a covalent double bond. Presuming a reaction mechanism similar to that of the bare atom, it appears that the covalent bonds to oxygen have little or no effect on the metal atom's ability to add to the alkene double bond and subsequently insert in the CH bond. The increase in rate from bare Zr to Zr(alkyne) could simply be a lifetime effect. The large addition to the number of degrees of freedom of the complex may discriminate against dissociation back to reactants, enhancing the elimination efficiency. Alternatively, it may be an electronic effect in which the ligand subtly lowers the barrier to CH insertion.

None of these first examples reveal any effect of steric hindrance by the ligand. The key common feature may be the availability of empty low-lying 4d orbitals of the proper symmetry to act as acceptors, allowing the ligated metal to form a strong bond to the alkene in all cases.

V. Conclusion

We have shown the feasibility and utility of 157 nm photoionization in determining the identity of metal-containing products of reactions of neutral transition-metal species. In Zr + alkene reactions, our results confirm theoretical predictions that H_2 elimination can occur over at most a small potential energy barrier. In addition to further applications to neutral product identification, the technique also holds great promise for extending kinetics studies to a variety of small ligated species, as demonstrated here for Zr(C_2H_2), Zr(C_3H_4), and ZrO.

Acknowledgment. We thank the National Science Foundation and the Donors of the Petroleum Research Foundation for generous support of this research. T.A.F. thanks Carleton

College for sabbatical support and the NSF for supplemental support during her leave in Madison.

References and Notes

(1) Armentrout, P. B.; Kickel, B. L. In *Organometallic Ion Chemistry*; Freiser, B. S., Ed.; Kluwer Academic Publishers: Dordrecht, The Netherlands, 1995.
(2) Weisshaar, J. C. *Acc. Chem. Res.* **1993**, *26*, 213.
(3) Eller, K.; Schwarz, H. *Chem. Rev.* **1991**, *91*, 1121.
(4) Ritter, D.; Carroll, J. J.; Weisshaar, J. C. *J. Phys. Chem.* **1992**, *96*, 10636.
(5) Carroll, J. J.; Weisshaar, J. C. *J. Am. Chem. Soc.* **1993**, *115*, 800.
(6) Carroll, J. J.; Haug, K. L.; Weisshaar, J. C. **1993**, *115*, 6962.
(7) Carroll, J. J.; Weisshaar, J. C. *J. Phys. Chem.* **1996**, *100*, 12355.
(8) Carroll, J. J.; Haug, K. L.; Weisshaar, J. C.; Blomberg, M. R. A.; Siegbahn, P. E. M.; Svensson, M. *J. Phys. Chem.* **1995**, *99*, 13955.
(9) Campbell, M. L. *Abstr. Pap.—Am. Chem. Soc.* **1998**, *215*, 314.
(10) Ritter, D.; Weisshaar, J. C. *J. Phys. Chem.* **1989**, *93*, 1576.
(11) Ritter, D.; Weisshaar, J. C. *J. Phys. Chem.* **1990**, *94*, 4907.
(12) Belyung, D. P.; Fontijn, A.; Marshall, P. *J. Phys. Chem.* **1993**, *97*, 3456.
(13) Slavejkov, A. G.; Stanton, C. T.; Fontijn, A. *J. Phys. Chem.* **1990**, *94*, 3347.
(14) Lian, L.; Mitchell, S. A.; Rayner, D. M. *J. Phys. Chem.* **1994**, *98*, 11637.
(15) Mitchell, S. A.; Hackett, P. A. *J. Chem. Phys.* **1990**, *93*, 7822.
(16) Lafleur, R. D.; Parnis, J. K.; Rayner, D. M. *J. Chem. Phys.* **1996**, *105*, 3551.
(17) Parnis, J. M.; Lafleur, R. D.; Rayner, D. M. *J. Phys. Chem.* **1995**, *99*, 673.
(18) Campbell, M. *J. Phys. Chem. A* **1997**, *101*, 9377.
(19) Matsui, R.; Senba, K.; Honma, K. *J. Phys. Chem. A* **1997**, *101*, 179.
(20) Willis, P. A.; Stauffer, H. U.; Hinrichs, R. Z.; Davis, F. *J. Chem. Phys.* **1998**, *108*, 2665.
(21) Carroll, J. J.; Weisshaar, J. C.; Siegbahn, P. E. M.; Wittborn, C. A. M.; Blomberg, M. R. A. *J. Phys. Chem.* **1995**, *99*, 14388.
(22) Blomberg, M. R. A.; Siegbahn, P. E. M.; Svensson, M.; Wennerberg, J. In *Energetics of organometallic species*; Martinho Simões, J. A., Ed.; Kluwer Academic Publishers: Dordrecht, 1992; p 387.
(23) Blomberg, M. R. A.; Siegbahn, P. E. M.; Nagashima, U.; Wennerberg, J. *J. Am. Chem. Soc.* **1991**, *113*, 424.
(24) Blomberg, M. R. A.; Siegbahn, P. E. M.; Svensson, M. *J. Phys. Chem.* **1992**, *96*, 9794.
(25) Siegbahn, P. E. M.; Blomberg, M. R. A. *J. Am. Chem. Soc.* **1992**, *114*, 10548.
(26) Siegbahn, P. E. M.; Blomberg, M. R. A.; Svensson, M. *J. Am. Chem. Soc.* **1993**, *115*, 1952.
(27) Rayner, D. M.; Lian, L.; Mitchell, S. A.; Hackett, P. A. *Surf. Rev. Lett.* **1996**, *3*, 675.
(28) Davis, F. Work in progress.
(29) Tonkyn, R.; Weisshaar, J. C. *J. Phys. Chem.* **1986**, *90*, 2305.
(30) Tonkyn, R.; Ronan, M.; Weisshaar, J. C. *J. Phys. Chem.* **1988**, *92*, 92.
(31) Wen, Y.; Rau, J.; Weisshaar, J. C. Manuscript in preparation.
(32) Wen, Y.; Yethiraj, A.; Weisshaar, J. *J. Chem. Phys.* **1997**, *106*, 5509.
(33) Moore, C. E. NBS Circular No. 467; U.S. Department of Commerce: Washington, DC., 1949; Vols. I—III.
(34) Sievers, M. R.; Jarvis, L. M.; Armentrout, P. B. *J. Am. Chem. Soc.* **1998**, *120*, 1891.
(35) Siegbahn, P. E. M.; Blomberg, M. R. A. *J. Am. Chem. Soc.* **1992**, *114*, 10548.
(36) Langhoff, S. R.; Bauschlicher, C. W., Jr. *Annu. Rev. Phys. Chem.* **1988**, *39*, 181.
(37) Yi, S. S.; Blomberg, M. R. A.; Siegbahn, P. E. R.; Weisshaar, J. C. *J. Phys. Chem. A* **1998**, *102*, 395.